Fermi National Accelerator Laboratory

Limits on the Anomalous ZZγ and Z$\gamma\gamma$ Couplings in p$\bar{\text{p}}$ Collisions at $\sqrt{s}$ = 1.8 TeV

S. Abachi et al.

The D0 Collaboration

Fermi National Accelerator Laboratory
P.O. Box 500, Batavia, Illinois 60510

July 1995

Disclaimer

Limits on the Anomalous $ZZ\gamma$ and $Z\gamma\gamma$ Couplings in $p\bar{p}$ Collisions at $\sqrt{s} = 1.8$ TeV

The DØ Collaboration[1]

(July 1995)

We performed a direct search for the anomalous $ZZ\gamma$ and $Z\gamma\gamma$ couplings by studying $p\bar{p} \to \ell\ell\gamma + X$, $(\ell = e, \mu)$ events at $\sqrt{s} = 1.8$ TeV with the DØ detector at the Fermilab Tevatron Collider. A fit to the transverse energy spectrum of the photon in the signal events, based on the data set corresponding to an integrated luminosity of 14.3 pb^{-1} (13.7 pb^{-1}) for the electron (muon) channel, yields the following 95% confidence level limits on the anomalous CP-conserving $ZZ\gamma$ couplings: $|h_{30}^Z| < 1.8$ $(h_{40}^Z = 0)$, and $|h_{40}^Z| < 0.5$ $(h_{30}^Z = 0)$, for a form-factor scale $\Lambda = 500$ GeV. Limits for the $Z\gamma\gamma$ couplings and CP-violating couplings are also discussed.

S. Abachi,[12] B. Abbott,[34] M. Abolins,[23] B.S. Acharya,[41] I. Adam,[10] D.L. Adams,[35] M. Adams,[15] S. Ahn,[12] H. Aihara,[20] J. Alitti,[37] G. Álvarez,[16] G.A. Alves,[8] E. Amidi,[27] N. Amos,[22] E.W. Anderson,[17] S.H. Aronson,[3] R. Astur,[39] R.E. Avery,[29] A. Baden,[21] V. Balamurali,[30] J. Balderston,[14] B. Baldin,[12] J. Bantly,[4] J.F. Bartlett,[12] K. Bazizi,[7] J. Bendich,[20] S.B. Beri,[32] I. Bertram,[35] V.A. Bezzubov,[33] P.C. Bhat,[12] V. Bhatnagar,[32] M. Bhattacharjee,[11] A. Bischoff,[7] N. Biswas,[30] G. Blazey,[12] S. Blessing,[13] P. Bloom,[5] A. Boehnlein,[12] N.I. Bojko,[33] F. Borcherding,[12] J. Borders,[36] C. Boswell,[7] A. Brandt,[12] R. Brock,[23] A. Bross,[12] D. Buchholz,[29] V.S. Burtovoi,[33] J.M. Butler,[12] D. Casey,[36] H. Castilla-Valdez,[9] D. Chakraborty,[39] S.-M. Chang,[27] S.V. Chekulaev,[33] L.-P. Chen,[20] W. Chen,[39] L. Chevalier,[37] S. Chopra,[32] B.C. Choudhary,[7] J.H. Christenson,[12] M. Chung,[15] D. Claes,[39] A.R. Clark,[20] W.G. Cobau,[21] J. Cochran,[7] W.E. Cooper,[12] C. Cretsinger,[36] D. Cullen-Vidal,[4] M.A.C. Cummings,[14] D. Cutts,[4] O.I. Dahl,[20] K. De,[42] M. Demarteau,[12] R. Demina,[27] K. Denisenko,[12] N. Denisenko,[12] D. Denisov,[12] S.P. Denisov,[33] W. Dharmaratna,[13] H.T. Diehl,[12] M. Diesburg,[12] G. Di Loreto,[23] R. Dixon,[12] P. Draper,[42] J. Drinkard,[6] Y. Ducros,[37] S.R. Dugad,[41] S. Durston-Johnson,[36] D. Edmunds,[23] J. Ellison,[7] V.D. Elvira,[12,‡] R. Engelmann,[39] S. Eno,[21] G. Eppley,[35] P. Ermolov,[24] O.V. Eroshin,[33] V.N. Evdokimov,[33] S. Fahey,[23] T. Fahland,[4] M. Fatyga,[3] M.K. Fatyga,[36] J. Featherly,[3] S. Feher,[39] D. Fein,[2] T. Ferbel,[36] G. Finocchiaro,[39] H.E. Fisk,[12] Yu. Fisyak,[24] E. Flattum,[23] G.E. Forden,[2] M. Fortner,[28] K.C. Frame,[23] P. Franzini,[10] S. Fuess,[12] A.N. Galjaev,[33] E. Gallas,[42] C.S. Gao,[12,*] S. Gao,[12,*] T.L. Geld,[23] R.J. Genik II,[23] K. Genser,[12] C.E. Gerber,[12,§] B. Gibbard,[3] V. Glebov,[36] S. Glenn,[5] B. Gobbi,[29] M. Goforth,[13] A. Goldschmidt,[20] B. Gómez,[1] P.I. Goncharov,[33] H. Gordon,[3] L.T. Goss,[43] N. Graf,[3] P.D. Grannis,[39] D.R. Green,[12] J. Green,[28] H. Greenlee,[12] G. Griffin,[6] N. Grossman,[12] P. Grudberg,[20] S. Grünendahl,[36] W. Gu,[12,*] G. Guglielmo,[31] J.A. Guida,[39] J.M. Guida,[3] W. Guryn,[3] S.N. Gurzhiev,[33] P. Gutierrez,[31] Y.E. Gutnikov,[33] N.J. Hadley,[21] H. Haggerty,[12] S. Hagopian,[13] V. Hagopian,[13] K.S. Hahn,[36] R.E. Hall,[6] S. Hansen,[12] R. Hatcher,[23] J.M. Hauptman,[17] D. Hedin,[28] A.P. Heinson,[7] U. Heintz,[12] R. Hernández-Montoya,[9] T. Heuring,[13] R. Hirosky,[13] J.D. Hobbs,[12] B. Hoeneisen,[1,¶] J.S. Hoftun,[4] F. Hsieh,[22] Ting Hu,[39] Tong Hu,[16] T. Huehn,[7] S. Igarashi,[12] A.S. Ito,[12] E. James,[2] J. Jaques,[30] S.A. Jerger,[23] J.Z.-Y. Jiang,[39] T. Joffe-Minor,[29] H. Johari,[27] K. Johns,[2] M. Johnson,[12] H. Johnstad,[40]

A. Jonckheere,[12] M. Jones,[14] H. Jöstlein,[12] S.Y. Jun,[29] C.K. Jung,[39] S. Kahn,[3] G. Kalbfleisch,[31]
J.S. Kang,[18] R. Kehoe,[30] M.L. Kelly,[30] A. Kernan,[7] L. Kerth,[20] C.L. Kim,[18] S.K. Kim,[38]
A. Klatchko,[13] B. Klima,[12] B.I. Klochkov,[33] C. Klopfenstein,[39] V.I. Klyukhin,[33]
V.I. Kochetkov,[33] J.M. Kohli,[32] D. Koltick,[34] A.V. Kostritskiy,[33] J. Kotcher,[3] J. Kourlas,[26]
A.V. Kozelov,[33] E.A. Kozlovski,[33] M.R. Krishnaswamy,[41] S. Krzywdzinski,[12] S. Kunori,[21]
S. Lami,[39] G. Landsberg,[12] R.E. Lanou,[4] J-F. Lebrat,[37] A. Leflat,[24] H. Li,[39] J. Li,[42] Y.K. Li,[29]
Q.Z. Li-Demarteau,[12] J.G.R. Lima,[8] D. Lincoln,[22] S.L. Linn,[13] J. Linnemann,[23] R. Lipton,[12]
Y.C. Liu,[29] F. Lobkowicz,[36] S.C. Loken,[20] S. Lökös,[39] L. Lueking,[12] A.L. Lyon,[21]
A.K.A. Maciel,[8] R.J. Madaras,[20] R. Madden,[13] I.V. Mandrichenko,[33] Ph. Mangeot,[37] S. Mani,[5]
B. Mansoulié,[37] H.S. Mao,[12,*] S. Margulies,[15] R. Markeloff,[28] L. Markosky,[2] T. Marshall,[16]
M.I. Martin,[12] M. Marx,[39] B. May,[29] A.A. Mayorov,[33] R. McCarthy,[39] T. McKibben,[15]
J. McKinley,[23] T. McMahon,[31] H.L. Melanson,[12] J.R.T. de Mello Neto,[8] K.W. Merritt,[12]
H. Miettinen,[35] A. Milder,[2] A. Mincer,[26] J.M. de Miranda,[8] C.S. Mishra,[12]
M. Mohammadi-Baarmand,[39] N. Mokhov,[12] N.K. Mondal,[41] H.E. Montgomery,[12] P. Mooney,[1]
M. Mudan,[26] C. Murphy,[16] C.T. Murphy,[12] F. Nang,[4] M. Narain,[12] V.S. Narasimham,[41]
A. Narayanan,[2] H.A. Neal,[22] J.P. Negret,[1] E. Neis,[22] P. Nemethy,[26] D. Nešić,[4] D. Norman,[43]
L. Oesch,[22] V. Oguri,[8] E. Oltman,[20] N. Oshima,[12] D. Owen,[23] P. Padley,[35] M. Pang,[17] A. Para,[12]
C.H. Park,[12] Y.M. Park,[19] R. Partridge,[4] N. Parua,[41] M. Paterno,[36] J. Perkins,[42] A. Peryshkin,[12]
M. Peters,[14] H. Piekarz,[13] Y. Pischalnikov,[34] A. Pluquet,[37] V.M. Podstavkov,[33] B.G. Pope,[23]
H.B. Prosper,[13] S. Protopopescu,[3] D. Pušeljić,[20] J. Qian,[22] P.Z. Quintas,[12] R. Raja,[12]
S. Rajagopalan,[39] O. Ramirez,[15] M.V.S. Rao,[41] P.A. Rapidis,[12] L. Rasmussen,[39] A.L. Read,[12]
S. Reucroft,[27] M. Rijssenbeek,[39] T. Rockwell,[23] N.A. Roe,[20] P. Rubinov,[39] R. Ruchti,[30]
S. Rusin,[24] J. Rutherfoord,[2] A. Santoro,[8] L. Sawyer,[42] R.D. Schamberger,[39] H. Schellman,[29]
J. Sculli,[26] E. Shabalina,[24] C. Shaffer,[13] H.C. Shankar,[41] R.K. Shivpuri,[11] M. Shupe,[2]
J.B. Singh,[32] V. Sirotenko,[28] W. Smart,[12] A. Smith,[2] R.P. Smith,[12] R. Snihur,[29] G.R. Snow,[25]
S. Snyder,[39] J. Solomon,[15] P.M. Sood,[32] M. Sosebee,[42] M. Souza,[8] A.L. Spadafora,[20]
R.W. Stephens,[42] M.L. Stevenson,[20] D. Stewart,[22] D.A. Stoianova,[33] D. Stoker,[6] K. Streets,[26]
M. Strovink,[20] A. Taketani,[12] P. Tamburello,[21] J. Tarazi,[6] M. Tartaglia,[12] T.L. Taylor,[29]
J. Teiger,[37] J. Thompson,[21] T.G. Trippe,[20] P.M. Tuts,[10] N. Varelas,[23] E.W. Varnes,[20]
P.R.G. Virador,[20] D. Vititoe,[2] A.A. Volkov,[33] A.P. Vorobiev,[33] H.D. Wahl,[13] G. Wang,[13]
J. Wang,[12,*] L.Z. Wang,[12,*] J. Warchol,[30] M. Wayne,[30] H. Weerts,[23] F. Wen,[13] W.A. Wenzel,[20]
A. White,[42] J.T. White,[43] J.A. Wightman,[17] J. Wilcox,[27] S. Willis,[28] S.J. Wimpenny,[7]
J.V.D. Wirjawan,[43] J. Womersley,[12] E. Won,[36] D.R. Wood,[12] H. Xu,[4] R. Yamada,[12] P. Yamin,[3]
C. Yanagisawa,[39] J. Yang,[26] T. Yasuda,[27] C. Yoshikawa,[14] S. Youssef,[13] J. Yu,[36] Y. Yu,[38]
Y. Zhang,[12,*] Y.H. Zhou,[12,*] Q. Zhu,[26] Y.S. Zhu,[12,*] Z.H. Zhu,[36] D. Zieminska,[16] A. Zieminski,[16]
and A. Zylberstejn[37]

[1] Universidad de los Andes, Bogotá, Colombia
[2] University of Arizona, Tucson, Arizona 85721
[3] Brookhaven National Laboratory, Upton, New York 11973
[4] Brown University, Providence, Rhode Island 02912
[5] University of California, Davis, California 95616
[6] University of California, Irvine, California 92717
[7] University of California, Riverside, California 92521
[8] LAFEX, Centro Brasileiro de Pesquisas Físicas, Rio de Janeiro, Brazil
[9] CINVESTAV, Mexico City, Mexico
[10] Columbia University, New York, New York 10027
[11] Delhi University, Delhi, India 110007
[12] Fermi National Accelerator Laboratory, Batavia, Illinois 60510
[13] Florida State University, Tallahassee, Florida 32306
[14] University of Hawaii, Honolulu, Hawaii 96822

[15]University of Illinois at Chicago, Chicago, Illinois 60607
[16]Indiana University, Bloomington, Indiana 47405
[17]Iowa State University, Ames, Iowa 50011
[18]Korea University, Seoul, Korea
[19]Kyungsung University, Pusan, Korea
[20]Lawrence Berkeley Laboratory and University of California, Berkeley, California 94720
[21]University of Maryland, College Park, Maryland 20742
[22]University of Michigan, Ann Arbor, Michigan 48109
[23]Michigan State University, East Lansing, Michigan 48824
[24]Moscow State University, Moscow, Russia
[25]University of Nebraska, Lincoln, Nebraska 68588
[26]New York University, New York, New York 10003
[27]Northeastern University, Boston, Massachusetts 02115
[28]Northern Illinois University, DeKalb, Illinois 60115
[29]Northwestern University, Evanston, Illinois 60208
[30]University of Notre Dame, Notre Dame, Indiana 46556
[31]University of Oklahoma, Norman, Oklahoma 73019
[32]University of Panjab, Chandigarh 16-00-14, India
[33]Institute for High Energy Physics, 142-284 Protvino, Russia
[34]Purdue University, West Lafayette, Indiana 47907
[35]Rice University, Houston, Texas 77251
[36]University of Rochester, Rochester, New York 14627
[37]CEA, DAPNIA/Service de Physique des Particules, CE-SACLAY, France
[38]Seoul National University, Seoul, Korea
[39]State University of New York, Stony Brook, New York 11794
[40]SSC Laboratory, Dallas, Texas 75237
[41]Tata Institute of Fundamental Research, Colaba, Bombay 400005, India
[42]University of Texas, Arlington, Texas 76019
[43]Texas A&M University, College Station, Texas 77843

Direct measurement of the $ZZ\gamma$ and $Z\gamma\gamma$ trilinear gauge boson couplings is possible by studying $Z\gamma$ production in $p\bar{p}$ collisions at the Tevatron ($\sqrt{s} = 1.8$ TeV). In what follows these couplings will be denoted $ZV\gamma$, where $V = Z, \gamma$. The most general Lorentz and gauge invariant $ZV\gamma$ vertex is described by four coupling parameters, h_i^V, ($i = 1...4$) (1). Combinations of the CP-conserving (CP-violating) parameters h_3^V and h_4^V (h_1^V and h_2^V) correspond to the electric (magnetic) dipole and magnetic (electric) quadrupole transition moments of the $ZV\gamma$ vertex. In the Standard Model (SM), all the $ZV\gamma$ couplings vanish at the tree level. Non-zero (i.e. *anomalous*) values of the h_i^V couplings result in an increase of the $Z\gamma$ production cross section and change the kinematic distribution of the final state particles (2). Partial wave unitarity of the general $f\bar{f} \to Z\gamma$ process restricts the $ZV\gamma$ couplings uniquely to their vanishing SM values at asymptotically high energies (3). There-fore, the coupling parameters have to be modified by form-factors $h_i^V = h_{i0}^V/(1 + \hat{s}/\Lambda^2)^n$, where $\hat{s}$ is the square of the invariant mass of the $Z\gamma$ system, Λ is the form-factor scale, and h_{i0}^V are coupling values at the low energy limit ($\hat{s} \approx 0$) (2). Following Ref. (2) we assume $n = 3$ for $h_{1,3}^V$ and $n = 4$ for $h_{2,4}^V$. Such a choice yields the same asymptotic energy behavior for all the couplings. Unlike $W\gamma$ production where the form-factor effects do not play a crucial role, the Λ-dependent effects cannot be ignored in $Z\gamma$ production. This is due to the higher power of $\hat{s}$ in the vertex function, a direct consequence of the additional

Bose-Einstein symmetry of the $ZV\gamma$ vertices (2).

We present a measurement of the $ZV\gamma$ couplings using $p\bar{p} \to \ell\ell\gamma + X$ ($\ell = e, \mu$) events observed with the DØ detector during the 1992–1993 run, corresponding to an integrated luminosity of $14.3 \pm 0.8\,\mathrm{pb}^{-1}$ ($13.7 \pm 0.7\,\mathrm{pb}^{-1}$) for the electron (muon) data. Similar measurements were recently performed by CDF (4) and L3 (5).

The DØ detector, described in detail elsewhere (6), consists of three main systems. The calorimeter consists of uranium-liquid argon sampling detectors in central and two end cryostats, and provides near-hermetic coverage in pseudorapidity (η) for $|\eta| \leq 4.4$. The energy resolution of the calorimeter has been measured in beam tests (7) to be $15\%/\sqrt{E}$ for electrons and $50\%/\sqrt{E}$ for isolated pions, where E is in GeV. The calorimeter is read out in towers that subtend 0.1×0.1 in $\eta \times \phi$ (where ϕ is the azimuthal angle) and are segmented longitudinally into 4 electromagnetic (EM) and $4 - 5$ hadronic layers. In the third EM layer, at the EM shower maximum, the towers are more finely subdivided, subtending 0.05×0.05 in $\eta \times \phi$. Central and forward drift chambers are used to identify charged tracks for $|\eta| \leq 3.2$. The muon system consists of magnetized iron toroids with one inner and two outer layers of drift tubes, providing coverage for $|\eta| \leq 3.3$. The muon momentum resolution for central muons ($|\eta| < 1.0$) is determined to be $\delta(1/p)/(1/p) = 0.18(p-2)/p \oplus 0.008p$ (p in GeV/c), using $J/\Psi, Z \to \mu\mu$ events.

Candidates are selected by searching for events containing two isolated electrons (muons) with high transverse energy E_T (transverse momentum p_T), and an isolated photon. The $ee\gamma$ sample is selected from a trigger requiring two isolated EM clusters, each with $E_T \geq$ 20 GeV. An electron cluster is required to be within the fiducial region of the calorimeter ($|\eta| \leq 1.1$ in the central calorimeter (CC), or $1.5 \leq |\eta| \leq 2.5$ in the end calorimeters (EC)). Offline electron identification requirements are: (i) the ratio of the EM energy to the total shower energy must be > 0.9; (ii) the lateral and longitudinal shower shape must be consistent with an electron shower (8); (iii) the isolation variable of the cluster (I) must be < 0.1, where I is defined as $I = [E_{\mathrm{tot}}(0.4) - E_{\mathrm{EM}}(0.2)]/E_{\mathrm{EM}}(0.2)$, $E_{\mathrm{tot}}(0.4)$ is the total shower energy inside a cone defined by $\mathcal{R} = \sqrt{(\Delta\eta)^2 + (\Delta\phi)^2} = 0.4$, and $E_{\mathrm{EM}}(0.2)$ is the EM energy inside a cone of $\mathcal{R} = 0.2$; (iv) at least one of the two electron clusters must have a matching track in the drift chambers; and (v) $E_T > 25$ GeV for both electrons.

The $\mu\mu\gamma$ sample is selected from a trigger requiring an EM cluster with $E_T > 7$ GeV and a muon track with $p_T > 5$ GeV/c. A muon track is required to have $|\eta| \leq 1.0$ and must have: (i) hits in the inner drift-tube layer; (ii) a good overall track fit; (iii) bend view impact parameter < 22 cm; (iv) a matching track in the central drift chambers; and (v) minimum energy deposition of 1 GeV in the calorimeter along the muon path. The muon must be isolated from a nearby jet ($\mathcal{R}_{\mu-\mathrm{jet}} > 0.5$). At least one of the muon tracks is required to traverse a minimum length of magnetized iron ($\int B dl > 1.9$ Tm); it is also required that $p_T^{\mu_1} > 15$ GeV/c and $p_T^{\mu_2} > 8$ GeV/c.

The requirements for photon identification are common to both $ee\gamma$ and $\mu\mu\gamma$ samples. We require a photon transverse energy $E_T^\gamma > 10$ GeV and the same quality cuts as those on the electron, except that there must be no track pointing toward the calorimeter cluster. Additionally, we require that the separation between a photon and both leptons be $\Delta\mathcal{R}_{\ell\gamma} > 0.7$. This cut suppresses the contribution of the radiative $Z \to \ell\ell\gamma$ decays (2). The above selection criteria yield four $ee\gamma$ and two $\mu\mu\gamma$ candidates (see Table I). Figure 1 shows the E_T^γ distribution for these events. Three $ee\gamma$ and both $\mu\mu\gamma$ candidates have a three body invariant mass close to that of the Z and low separation between the photon and one of the leptons, consistent with the interpretation of these events as radiative $Z \to \ell\ell\gamma$ decays. The remaining $ee\gamma$ candidate has a dielectron mass compatible with that of the Z and a photon well separated from the leptons, an event topology typical for direct $Z\gamma$ production

in which a photon is radiated from one of the interacting partons (2).

The estimated background includes contributions from (*i*) $Z + \text{jet(s)}$ production where one of the jets fakes a photon or an electron (the latter case corresponds to the $ee\gamma$ signature if additionally one of the electrons from the $Z \rightarrow ee$ decay is not detected in a tracking chamber); (*ii*) QCD multijet production with jets being misidentified as electrons or photons; (*iii*) $\tau\tau\gamma$ production followed by decay of each τ to $\ell\overline{\nu}_\ell\nu_\tau$.

We estimate the QCD background from data using the probability, $P(\text{jet} \rightarrow e/\gamma)$, for a jet to be misidentified as an electron/photon. This probability is determined by measuring the fraction of non-leading jets in samples of QCD multijet events that pass our photon/electron identification cuts, and takes into account a 0.25 ± 0.25 fraction of direct photon events in the multijet sample (9). We find the misidentification probabilities $P(\text{jet} \rightarrow e/\gamma)$ to be $\sim 10^{-3}$ in the typical E_T ranges for the electrons and photons of between 10 and 50 GeV. We find the background from $Z + \text{jet(s)}$ and QCD multijet events in the electron channel by applying misidentification probabilities to the jet E_T spectrum of the inclusive $ee + \text{jet(s)}$ and $e\gamma + \text{jet(s)}$ data. For the muon channel the QCD background is estimated by applying the misidentification probability to the inclusive $\mu\mu + \text{jet(s)}$ spectrum. The estimation of the QCD background from data in the muon case also accounts for cosmic ray background. The $\tau\tau\gamma$ background is estimated using the ISAJET Monte Carlo (MC) event generator (10) followed by a full simulation of the DØ detector. The backgrounds for each channel are summarized in Table I.

Subtracting the estimated backgrounds from the observed number of events, the signal is $3.57^{+3.15}_{-1.91} \pm 0.06$ for the $ee\gamma$ channel and $1.95^{+2.62}_{-1.29} \pm 0.01$ for the $\mu\mu\gamma$ channel, where the first and dominant uncertainty is due to Poisson statistics, and the second is due to the systematic error of the background estimate.

The acceptance of the DØ detector for the $ee\gamma$ and $\mu\mu\gamma$ final states was studied using the leading order event generator of Baur and Berger (2) followed by a fast detector similation which takes into account resolution effects, variations in vertex position along the beam-axis, and trigger and offline efficiencies. These efficiencies are estimated using $Z \rightarrow ee$ data for the electron channel. The muon trigger efficiency is estimated from the $e\mu$ data selected using non-muon triggers. The offline efficiency for the muon channel is calculated based on $e\mu$ and $Z \rightarrow \mu\mu$ samples. The trigger efficiency for $ee\gamma$ is 0.98 ± 0.01 while the efficiency of offline dielectron identification is 0.64 ± 0.02 in the CC and 0.56 ± 0.03 in the EC. For the muon channel the trigger efficiency is $0.94^{+0.06}_{-0.09}$, and the offline dimuon identification efficiency is 0.54 ± 0.04. The photon efficiency depends on E_T^γ due to the calorimeter cluster shape algorithm and the isolation cut, and accounts for loss of the photon due to a random track overlap (which results in misidentification of the photon as an electron) and the photon conversion into an e^+e^- pair before the outermost tracking chamber. It grows by 82% over the E_T^γ range of 10 to 30 GeV, and is approximately constant above 30 GeV. The photon efficiency averaged over the SM E_T^γ spectrum (see Fig. 1) is 0.53 ± 0.05. The geometrical acceptances and overall efficiencies for two channels for the SM case are given in Table I. The MRSD$-'$ (11) set of structure functions (s.f.) is used in the calculations. The effect of higher order QCD corrections is accounted for by multiplying the rates by a constant factor $k = 1.34$ (2). The 7% uncertainty on the QCD corrections (choice of s.f., k-factor systematics) are included in the systematic error of the MC calculation.

We compare the observed number of events with the SM expectation (see Table I; the first and second errors are due to the uncertainty in the MC modelling and the integrated luminosity calculation, respectively) using the estimated efficiency and acceptance. They agree within the errors for both channels.

To set limits on the anomalous coupling parameters, we fit the observed E_T spectrum of the photon (E_T^γ) with the MC predictions plus the estimated background, combining the

information in the spectrum shape and the event rate. The fit is performed for the $ee\gamma$ and $\mu\mu\gamma$ samples, using a binned likelihood method (12), including constraints to account for our understanding of luminosity and efficiency uncertainties. Because the contribution of the anomalous couplings is concentrated in the high E_T^γ region, the differential distribution $d\sigma/dE_T^\gamma$ is more sensitive to the anomalous couplings than a total cross section (see insert in Fig. 1 and Ref. (2)). To optimize the sensitivity of the experiment for the low statistics, we assume Poisson statistics for each E_T^γ bin and use the maximum likelihood method to fit the experimental data. To exploit the fact that anomalous coupling contributions lead to an excess of events at high transverse energy of the photon, a high-E_T^γ bin, in which we observe no events is explicitly used in the histogram (12). The results were cross-checked using an unbinned likelihood fit which yields similar results.

Figure 1 shows the observed E_T^γ spectrum with the SM prediction plus the estimated background for the $e + \mu$ combined sample. The 95% confidence level (CL) limit contour for the CP-conserving anomalous coupling parameters h_{30}^Z and h_{40}^Z is shown in Fig. 2. A form-factor scale $\Lambda = 500$ GeV is used for the calculations of the experimental limits and partial wave unitarity constraints. We obtain the following 95% CL limits for the CP-conserving $ZZ\gamma$ and $Z\gamma\gamma$ couplings (in the assumption that all couplings except one are at the SM values, i.e. zeros):

$$-1.8 < h_{30}^Z < 1.8; \; -0.5 < h_{40}^Z < 0.5$$
$$-1.9 < h_{30}^\gamma < 1.9; \; -0.5 < h_{40}^\gamma < 0.5$$

The correlated limits for pairs of couplings (h_{30}^V, h_{40}^V) are less stringent due to the strong interference between these couplings:

$$-3.3 < h_{30}^Z < 3.3; \; -0.8 < h_{40}^Z < 0.8$$
$$-3.5 < h_{30}^\gamma < 3.4; \; -0.8 < h_{40}^\gamma < 0.8$$

Limits on the CP-violating $ZV\gamma$ couplings are numerically the same as those for the CP-conserving couplings. The limits on the h_{20}^Z, h_{40}^Z, and h_{i0}^γ couplings are currently the most stringent available.

Global limits on the anomalous couplings (i.e., limits independent of the values of other couplings) are close to the correlated limits for (h_{30}^V, h_{40}^V) and (h_{10}^V, h_{20}^V) pairs, since other possible combinations of couplings interfere with each other only at the level of 10%. This is illustrated in Fig. 3, which shows the limits for pairs of couplings of the same CP-parity (couplings with different CP-parity do not interfere with each other). Indeed, in the absence of correlations, any non-zero values of other couplings saturate the available phase space for the pair of couplings in Fig. 2. The global limits for this pair therefore correspond to the case when all other couplings are zero. Since there is a strong correlation between couplings in Fig. 2 the global limit for one coupling corresponds to the case when the other is not at zero.

We also study the form-factor scale dependence of the results. The chosen value of the scale $\Lambda = 500$ GeV is close to the sensitivity limit of this experiment for the $h_{20,40}^V$ couplings: for larger values of the scale partial wave unitarity is violated for certain values of anomalous couplings allowed at 95% CL by this measurement.
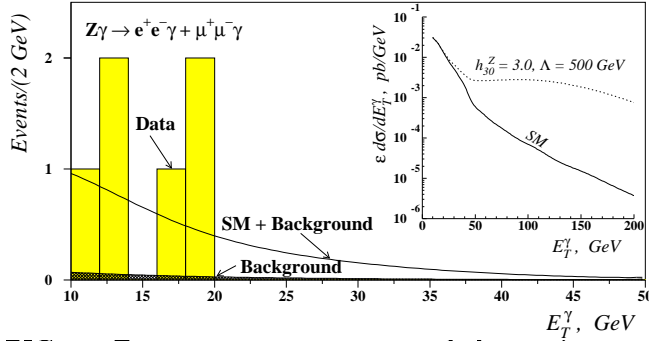
FIG. 1. Transverse energy spectrum of photons in $ee\gamma$ and $\mu\mu\gamma$ events. The shadowed bars correspond to data points, the hatched curve represents the total background, and the solid line shows the sum of the SM predictions and the background. The insert shows $d\sigma/dE_T^\gamma$ folded with the efficiencies for SM and anomalous ($h_{30}^Z = 3.0$) couplings.

REFERENCES

* Visitor from IHEP, Beijing, China.

‡ Visitor from CONICET, Argentina.

§ Visitor from Universidad de Buenos Aires, Argentina.

¶ Visitor from Univ. San Francisco de Quito, Ecuador.

1. K. Hagiwara *et al.*, Nucl. Phys. **B282**, 253 (1987).
2. U. Baur and E.L. Berger, Phys. Rev. **D47**, 4889 (1993).
3. K. Hagiwara and D. Zeppenfeld, Nucl. Phys. **B274**, 1 (1986); U. Baur and D. Zeppenfeld, Phys. Lett. **201B**, 383 (1988).
4. F. Abe *et al.* (CDF Collaboration), preprint Fermilab–Pub–94/304–E, Phys. Rev. Lett. (in print).
5. M. Acciarri *et al.* (L3 Collaboration), preprint CERN–PPE/94–216, Phys. Lett. **B** (in print).
6. S. Abachi *et al.* (DØ Collaboration), Nucl. Instrum. Methods **A338**, 185 (1994).
7. S. Abachi *et al.* (DØ Collaboration), Nucl. Instrum. Methods **A324**, 53 (1993); H. Aihara *et al.* (DØ Collaboration), Nucl. Instrum. Methods **A325**, 393 (1993).
8. M. Narain (DØ Collaboration), "Proceedings of the APS/DPF Conference", Fermilab (1992), eds. R. Raja and J. Yoh; R. Engelmann *et al.*, Nucl. Instrum. Methods **A216**, 45 (1983).
9. S. Fahey (DØ Collaboration), to appear in the "Proceedings of the APS/DPF Conference", Albuquerque, (1994).
10. F. Paige and S. Protopopescu, BNL Report no. BNL–38034, 1986 (unpublished), release V6.49.
11. A.D. Martin, R.G. Roberts and W.J. Stirling, Phys. Lett. **306B** 145 (1993); Erratum, Phys. Lett. **309B** 492 (1993).
12. G. Landsberg, in Proc. Workshop on Physics at Current Accelerators and the Supercollider, ANL–HEP–CP–93-92, 303 (1992); Ph.D. Dissertation, SUNY at Stony Brook (1994), unpublished.
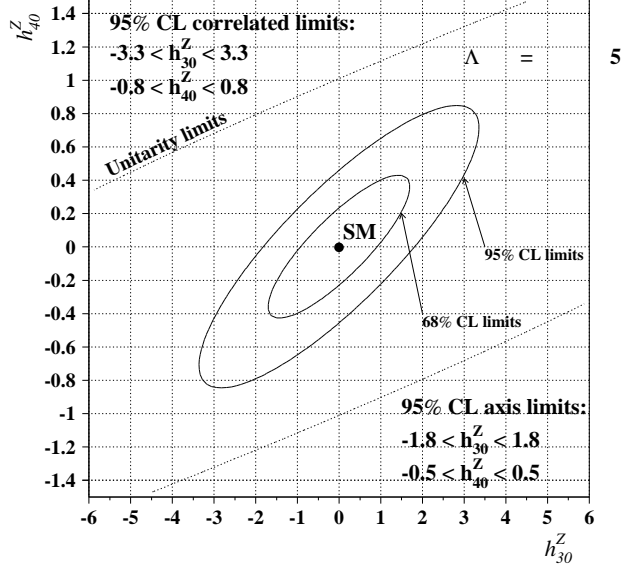
FIG. 2. Limits on the correlated CP-conserving anomalous $ZZ\gamma$ coupling parameters h_{30}^Z and h_{40}^Z. The solid ellipses represent 68% and 95% CL exclusion contours. The dashed curve shows limits from partial wave unitarity for $\Lambda = 500$ GeV.

TABLE 1. Summary of signal and backgrounds.

Channel	$ee\gamma$	$\mu\mu\gamma$
Candidates	4	2
QCD background	0.43 ± 0.06	0.02 ± 0.01
$\tau\tau\gamma$ background	0.004 ± 0.002	0.03 ± 0.01
Total background	0.43 ± 0.06	0.05 ± 0.01
Signal	$3.57^{+3.15}_{-1.91} \pm 0.06$	$1.95^{+2.62}_{-1.29} \pm 0.01$
Geometrical acceptance	53%	20%
Overall efficiency	0.17 ± 0.02	0.06 ± 0.01
SM predictions	$2.8 \pm 0.3 \pm 0.2$	$2.3 \pm 0.4 \pm 0.1$
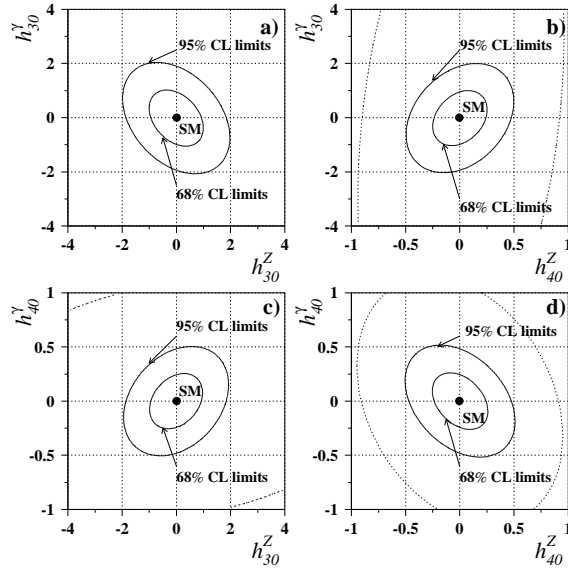
FIG. 3. Limits on the weakly correlated CP-conserving pairs of anomalous $ZV\gamma$ couplings: a) $(h_{30}^Z, h_{30}^\gamma)$, b) $(h_{40}^Z, h_{30}^\gamma)$, c) $(h_{30}^Z, h_{40}^\gamma)$, and d) $(h_{40}^Z, h_{40}^\gamma)$. The solid ellipses represent 68% and 95% CL exclusion contours. Dashed curves show limits from partial wave unitarity for $\Lambda = 500$ GeV.